Dynamics of Hydration of Nanocellulose Films

*Paolo Bettotti, Cecilia Ada Maestri, Romain Guider, Ines Mancini, Einat Nativ-Roth, Yuval Golan, and Marina Scarpa**

The design of materials capable of mechanical responses to physical and chemical stimuli represents one of the most exciting and challenging areas of scientific research because of the huge number of their potential applications. This article is focused on the molecular events occurring in thin films of carboxylated nanocellulose fibers, which are capable of converting water gradients into mechanical movements at the macroscopic scale. The analysis of the mechano-actuation, and of the conditions to obtain it, shows that the film movement is fast and reproducible, the gradient intensity is transduced into rate of displacement, and the response is observed at vapor pressures as low as 1.2 mm Hg. The actuation mechanism is associated to an efficient and reversible water sorption process by the hydrophilic nanocellulose fibers at the film interface. Conversely, water desorption is slow and follows a kinetic behavior supporting the presence of two binding sites for water molecules. The adsorbed water induces swelling of the surface nanocellulose layers and local structural rearrangement, however transitions between ordered and random coil conformations are not observed. The understanding of the actuation mechanisms of nanocellulose offers exciting opportunities to design macroscopic structures responding to chemical gradients by the assembly of simple molecular components.

1. Introduction

Nature has developed several actuators, spanning from nano to macroscale dimensions, such as Adenosine Triphosphate synthases (ATPases) or mammalian muscles. These biomolecular motors have inspired many attempts to realize artificial machineries activated by specific stimuli. The design and construction of artificial dynamic material systems able to sense, interact, adapt, and respond to the surrounding environment is, thus, a great scientific pursuit.[1–8] Stimuli responsive materials (also termed smart materials) is a broad class of materials that try to mimic the complex functionalities of living systems and are able to respond to a large variety of stimuli (such as electric, magnetic, photonic, thermic, and pH/solvent changes). Among the very broad types of materials and approaches currently investigated, those that use water to induce changes of the conformations of the molecular components are of particular interest because of their possible uses in bio-applications.[9–13] Hydrogels, a cross-linked polymer in contact with an aqueous environment, are among the most investigated materials because of their ease of fabrication and large tunability of their properties and are used to translate a chemical signal into a mechanical output in the form of a reversible change of the gel volume.[14,15] The swelling of the hydrogel might be used to induce a further action, for example to bend microstructures[16] or to create autonomous self-oscillating systems.[17] Other natural examples of such actuation can be found in vegetables and can be used to design artificial analogous with a predetermined mechanical behavior.[18,19] For example "active" movements can be found in the Venus flytrap, which closes its leaves in milliseconds to capture preys. On the other hand, "passive" actuation is the one determined by the hygroscopic movements of pine cones, wheat awns, and ice plant seed capsules.

Thus, despite being known since centuries, cellulose is still on the limelight thanks to the broad types of actuation mechanisms that it sustains, piezo effect and electro-active paper,[20–22] which were recently demonstrated. Moreover once the cellulose fibrils are reduced to nanometer scale, its optical and mechanical properties are heavily affected and can be tuned to a large extent.[23,24]

In this paper, we report about the mechanical response of oxidized nanofibrillated cellulose (NC) films exposed to water

Dr. P. Bettotti, C. A. Maestri,
Dr. R. Guider, Prof. M. Scarpa
Nanoscience Laboratory
Department of Physics
University of Trento
Via Sommarive 14, 38123 Povo, TN, Italy
E-mail: marina.scarpa@unitn.it

Prof. I. Mancini
Bioorganic Chemistry Laboratory
Department of Physics
University of Trento
Via Sommarive 14, 38123 Povo, TN, Italy

Dr. E. Nativ-Roth, Prof. Y. Golan
Department of Materials Engineering
Ben Gurion University of the Negev
Beer Sheva 84105, Israel

Prof. Y. Golan
Ilse Katz Institute for Nanoscale
Science and Technology
Ben Gurion University of the Negev
Beer Sheva 84105, Israel

Prof. M. Scarpa
Istituto Nazionale Biostrutture Biosistemi
Viale delle medaglie d'oro
Rome 00100, Italy

DOI: 10.1002/admi.201500415

fluxes. These films reversibly transduce a water gradient into a fast and reversible bending movement. The actuation responds to water gradients, but it does not respond to gradients of nonpolar solvents and is scarcely activated by polar organic solvents such as ethanol or acetone. The bending movement follows the direction of the water molecules flux and its rate is quantitatively dependent on the magnitude of this flux.

The increasing interest in moisture-responsive materials made of cellulose and of its derivatives is supported by the recent publications of Zhang et al.[25] and Wang et al.[26] The first paper reports an investigation of the reversible shape transitions of films of cellulose stearoyl esters, the second describes the phenomenological basics of the nanocellulose actuation but without shining light on the origin of this effect. In the present paper, we investigated the dynamics of the interaction between NC films and a flux of gaseous water molecules which generates a fast, reversible, and powerful bending movement. The film quantitatively converts the intensity of the gaseous water flux into rate of bending. We focused on the microscopic events underlying the actuation and demonstrated that the adsorbed water induces structural rearrangement of the film associated to interfacial fibers, most probably driven by electrostatic interactions. The understanding of these basic mechanisms would improve the fabrication of fiber-like cellulose-based actuation devices.

2. Film Structure, Morphology, and Structural Modifications due to Water Vapor Absorption

Transmission electron microscope (TEM) images of the nanocellulose fibers deposited over a TEM grid from the aqueous nanocellulose suspension are shown in **Figure 1**a,b. The straight form of the fibers support the model of cellulose fibers made of crystalline domains bound by flexible and amorphous domains.[27] The latter show a much larger reactivity toward oxidation and are broken upon sonication.[28] Few bent domains are still present after sonication and are highlighted in the TEM images.

Fiber sizes were characterized by statistical analysis on several TEM images and the typical length and width of the whiskers are reported in Figure 1c. Fiber width is centered at about 4 nm and this size is compatible with that of an elementary fibril of wood cellulose nanocrystals.[29] Interestingly, similar average fiber dimensions have been obtained from the lateral profiles of the Atomic Force Microscopy (AFM) images of NC films, thus suggesting that the fibers are not heavily entangled in 3D and that the film tends to grow with a layer-by-layer structure (data shown in Figures SI2 and SI3 in the Supporting Information).

Because of the small size of the nanofibers, the dry films are transparent in the visible range and their Fourier Transform Infrared (FTIR) spectrum (Figure SI4, Supporting Information) shows the characteristic features of the cellulose fibrils[30] together with the strong peak at 1609 cm^{-1} ascribable to the carboxylate vibration. The absorption of water vapor by NC films was monitored by FTIR using heavy water, the vibrational features of which are easily distinguishable in the NC spectrum.

The dynamics of the D_2O exchange with the NC film is shown in **Figure 2**a: both OH (squares) as well as OD (circle) bands were monitored with FTIR. Upon exposure to heavy water vapor, the typical band at 2504 cm^{-1} develops[31] in a spectrum region free of other signals and attributable to OD stretching. The OH stretching band at 3345 cm^{-1} is almost unchanged during this process and this fact suggests a negligible contribution of labile hydroxyls undergoing hydrogen–deuterium exchange and agrees with the TEM images showing of a nearly completely crystalline phase of the nanofibers.[32]

The absorption of D_2O is very fast; the absorption band reaches a steady intensity after two minutes of exposure (obtained by keeping a sessile drop hanging over the film) as shown in Figure 2b. On the other hand desorption is a slow process that requires hours to complete as shown in the right curve of Figure 2b. The desorption kinetics were analyzed assuming that two parallel independent first order kinetic processes are present, related to two different water binding sites.[33] Accordingly, the experimental data of Figure 2b were fitted to the equation

$$I_t = I_1 e^{-t/\tau_1} + I_2 e^{-t/\tau_2} \tag{1}$$

where I_t is the signal intensity at any time, the subscripts 1 and 2 refer to the desorption processes occurring at the two binding sites, I_1 and I_2 are the signal intensities when all the sites are

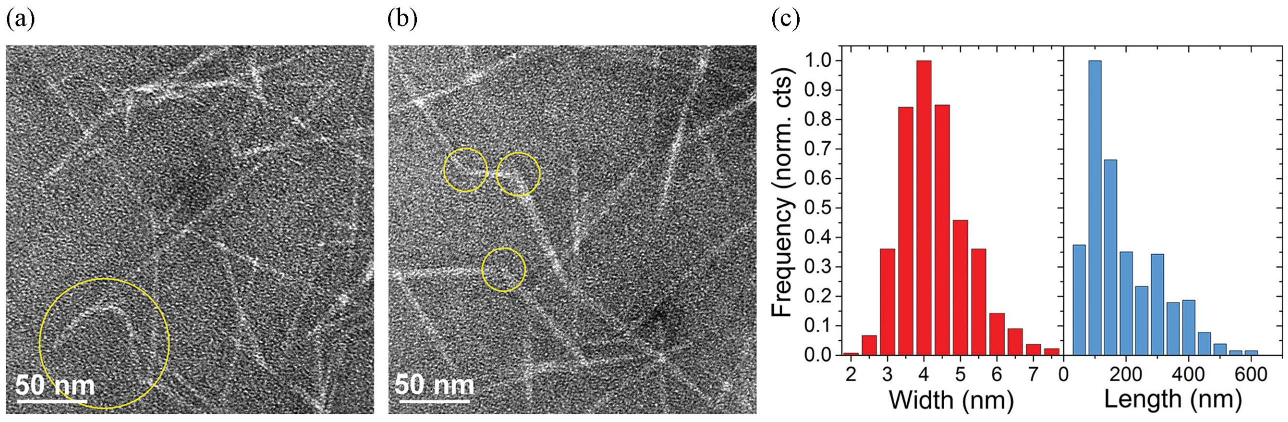

Figure 1. a,b) TEM views of NC fibrils. The circles highlight some of the rare flexible domains joining adjacent cellulose nanocrystals. Scale bar: 50 nm. c) Statistical distribution of fiber width (left panel) and length (right panel).

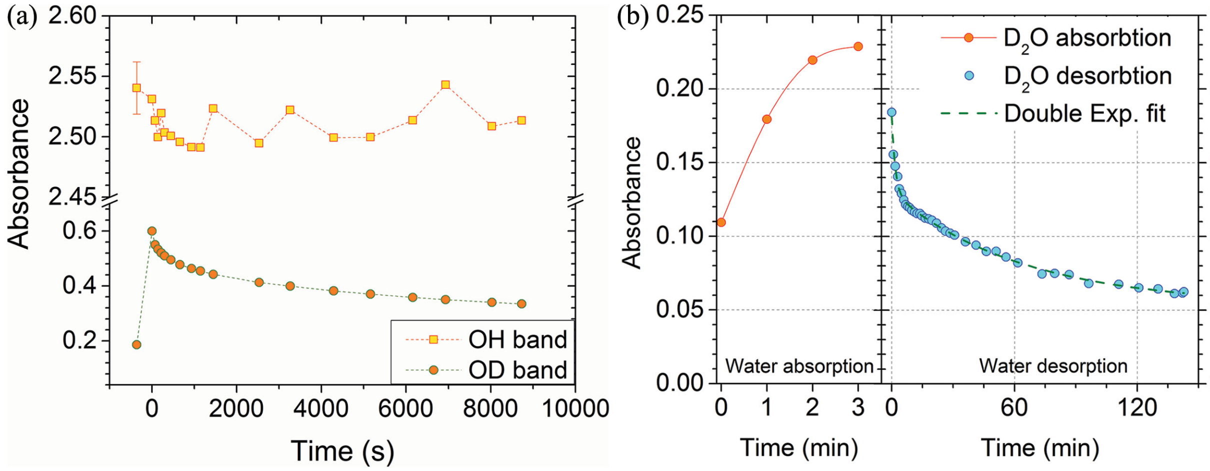

Figure 2. a) Dynamic of D_2O desorption. Both OH (3345 cm^{-1}) and OD (2504 cm^{-1}) groups were monitored using FTIR. The OD band shows a clear reduction of the absorbance with time (corresponding to an increase of transmittance of 84%) while the intensity of the OH peak remains almost constant (transmittance oscillations are <0.1%). b) Dynamics of both absorption (left) and desorption (right) of D_2O from NC film.

saturated. The desorption kinetic data were satisfactorily fitted to Equation (1), and we obtained the values of 1.7 and 63 min for the exponential time constants τ_1 and τ_2, respectively (mean value $\tau_1 = (2.2 \pm 0.9)$ min and $\tau_2 = (50 \pm 24)$ min calculated by a set of four replicated experiments using different NC films). These values agree with the data of Belbekhouche et al.[34] who measured the water desorption from nanocellulose by dynamic gravimetry and of Kohler et al.[35] who used a similar approach to monitor the behavior of flax cellulose fibers. These two works report on the variation of the water content of the sample, while by FTIR analysis we monitor all the O–D groups, including the saccharide hydroxyls undergoing hydrogen–deuterium exchange. The fast and almost undetectable decrease of the OH band at 3350 cm^{-1} (see Figure 2a) upon saturation with D_2O indicates a negligible contribution of labile hydroxyls to the observed phenomenon and, as a consequence, the time course of the peak at 2500 cm^{-1} essentially monitors the D_2O sorption/desorption capacity of NC. Some authors suggested that this H–D exchange is due to the O–3D...O–5 bond.[36]

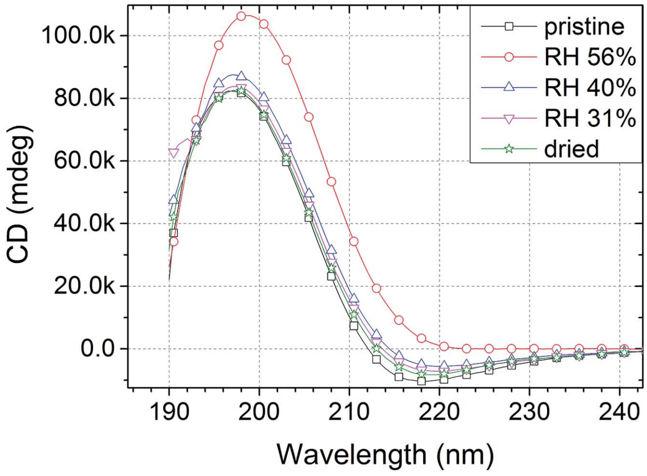

Figure 3. CD of NC film for different values of RH. The large positive ellipticity at 198 nm is due to the carboxylic group.

An approximate value of the total amount of D_2O absorbed by the NC film was calculated by the FTIR absorbance, by assuming that the Lambert–Beer law holds and considering $\varepsilon_{2500} = 69.69$ M^{-1} cm^{-1}.[37] In this way, we could estimate that after exposing the film to D_2O until saturation, the D_2O concentration in the film is as high as 6 M, that is, an upper limit of 30 µg of D_2O can be absorbed by a film with a 5 mm × 5 mm × 10 µm size (corresponding to around 8% in mass).

Exposure of the film to water vapors induces modifications of the structure of the NC fibers as shown by the Circular Dichroism (CD) spectra of the film reported in **Figure 3**. The CD spectrum of the film recorded under dried nitrogen atmosphere (black curve) shows a dispersive feature with a large positive ellipticity at 198 nm and a shallow negative signal at 218 nm. This ellipticity profile has been observed in gellan solutions[38] and carboxylated agarose,[39] where in both cases it has been associated to the presence of the carboxylic group. The spectra recorded at different relative humidity (RH), by equilibration of the optical cell compartment with a variable nitrogen/water vapor flow show a progressive increase of the positive peak at 198 nm accompanied by the disappearance of the negative contribution. A similar spectral modification was observed when gellan solutions are cooled.[40] The NC films stored in a desiccator over silica gel are flat and almost straight and retain their shape when exposed to uniform damp atmosphere (humidity up to 80%). However, if the dry film is laid over a water droplet, it shows an apparent hydrophobic repulsion and bends to keep the exposed side far from the water droplet (Movie S1, Supporting Information). Polar solvents such as ethanol induce a modest and slow bending while nonpolar solvents such as toluene are completely ineffective. Due to the very hydrophilic NC nature and the spectroscopic (FTIR and CD) data, the film actuation could be ascribed to a structural modification induced by the sorption of the water vapor molecules by the NC fibers. To monitor possible modifications of the fiber position due to water adsorption, we performed AFM analysis on the same film area before and after wetting of the film. This analysis shows that the single NC fibers keep their relative position and their relative (random) alignment (experimental details and results in the Supporting Information, Section "Monitoring of the fiber position before and after wetting a NC film"). However, we noticed a systematically positive displacement of the selected sections of the film which can be the signature of a planar overall expansion of the film layers exposed to water molecules.

The film movement is reversible, i.e., the film recovers a flat shape if exposed back to air and by turning upside down the bent film, it reverses the direction of bending. Both the film sides show the same bending capacity, suggesting that the film surface is isotropic and the two sides undergo similar interaction with the water molecules diffusing over or inside the film. The film senses the direction of the flux of evaporating water molecules and bends its free end accordingly, as shown in Movie S2 (Supporting Information) where films with two hanging ends are laid over a water reservoir.

The bending of the film has been monitored in real time to characterize both the extent and the kinetics of actuation, under controlled experimental conditions, since the exposure of the film to the fluid drop, by the setup shown in the Experimental Section. Repeated exposure of the film to water by opening and closing the shutter for 15 and 20 s, respectively, produces a reduction of the maximum bending angle. The reduction extent varies for different films (as reported later on). However, the bending capacity is fully recovered if the same film is left to dry for a few hours and then repeatedly exposed again to water. Also in this case, the delayed recovering of the film performance is in line with the FTIR data which show a fast D_2O sorption by NC and a desorption process occurring in more than 2 h. The highly reproducible interaction with water vapor of the dried films was confirmed by measuring the response of 18 films (10 × 10 mm in size and a thickness of 8, 10, 13, 15, 17, and 19 µm, three films for each thickness value). Each film was tested three times waiting 6 h before testing each film again, to allow full water desorption. **Figure 4**a plotted the maximum bending angle as function of film thickness. Each experimental point of this figure is the mean of nine bending angle values: three films, tested three times each, details in Figure SI5 (Supporting Information). The maximum bending angle (MBA) is independent of the film thickness until about 14 µm, while a progressive reduction is observed for larger thickness values (50% reduction by a factor of two increase in thickness). The bending angle decreases at higher ambient humidity. This is quite obvious since ambient water vapor should saturate homogeneously the water binding sites which are not anymore available to respond to the water flux. MBA slightly increases by increasing the film size until about 0.5 × 0.5 cm then it becomes almost independent of size (Figures SI6 and SI7, Supporting Information).

The bending kinetics are diffusion limited, as we demonstrated performing experiments at variable vapor fluxes. In these experiments, the same film was exposed to fluid drops containing ethylene glycol at variable percentage by weight in water. Ethylene glycol contributes negligibly to the vapor pressure (its vapor pressure is 7 Pa at 22 °C), so that the vapor pressure at the gas/liquid interphase depends on the water content of the fluid drop. If Fickian diffusion occurs, variable fluxes of water molecules interact with the NC film surface. MBA appears vapor pressure independent but the response time increases inversely with the vapor pressure for pressures below 14 mm Hg (as shown in Figure 4b). The effect is very remarkable since the time is 2–3 s at 100% water and about 70 min at 2% water. However, even at the lowest water concentration tested (1.2 mm Hg vapor pressure, corresponding to 60×10^{-3} M water molecules in the gas phase in contact with the water drop) the actuation mechanism occurs. It is notable that the MBA does not depend on the partial pressure of water and is rather constant. The effect of temperature was investigated exposing the film to water drops kept at different temperatures. The increase in temperature results in an increased pressure of the water vapor in equilibrium with the droplet, which can be calculated according to the Antoine equation. However, thermal convection and hot water vapors should produce a temperature gradient along the film thickness. Interestingly, in this case we

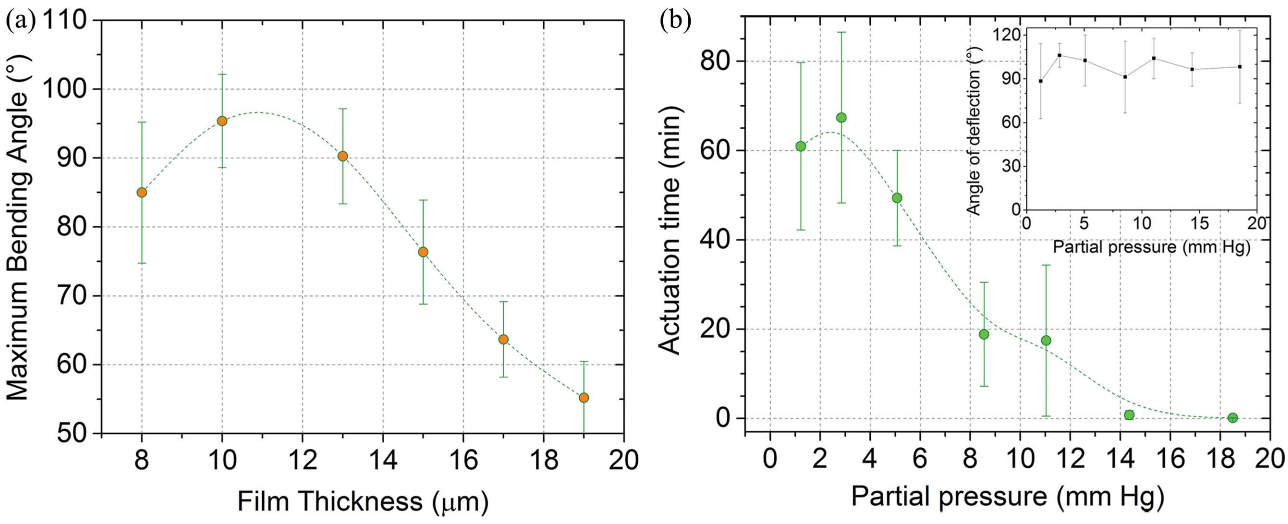

Figure 4. a) Maximum bending angle for different film thickness. The error bars are the standard deviation over a set of three measurements. The ambient humidity was 25% during all the 54 measurements used to obtain this plot. b) Actuation time as a function of the water partial pressure. The inset shows that the MBA is insensitive to the partial pressure of the water.

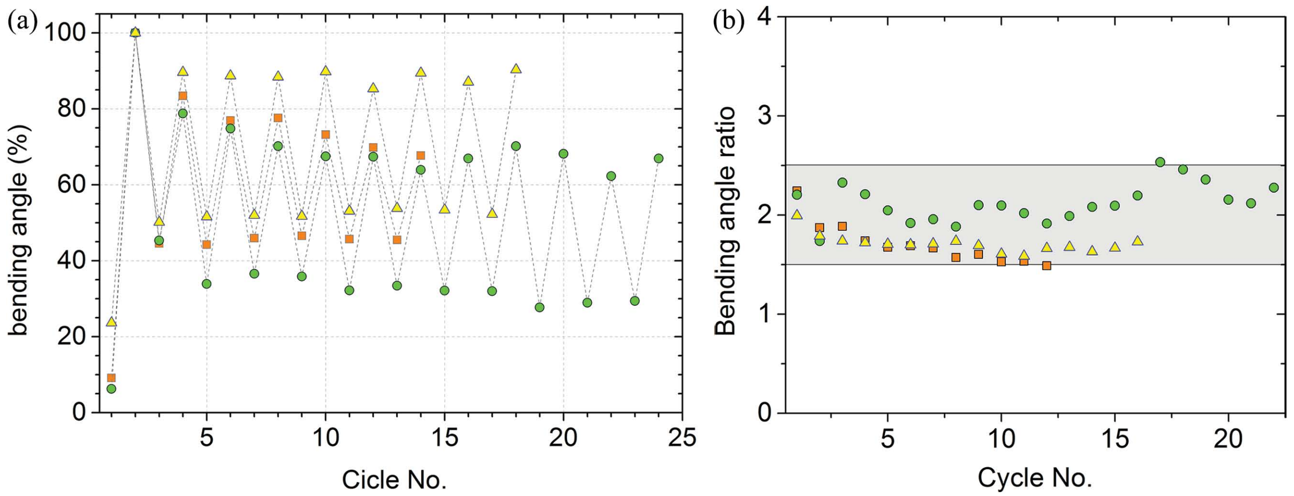

Figure 5. Reproducibility of the film actuation. a) Bending angle of different films subjected to repeated cycles of actuation. The first point refers to the rest position of the film. b) Ratio between bending angles reached in consecutive actuations.

observed both, an increase of the bending rate with increasing temperature, but also an increase of the bending angle, as shown in Figure S18 (Supporting Information).

Preliminary results show that the actuation is apparently induced also by a temperature gradient if the film is exposed to a cold surface, such as a wire kept at liquid nitrogen temperature. However we noticed that the film exposed to a hot surface (an incandescent metallic heater) did not show any bending (data not shown).

The bending of the films is highly reproducible and only a limited viscoelastic behavior is typically shown by the films. **Figure 5** reports the bending (as a percentage of the maximum bending angle) repeated over tens of cycles. Each film was exposed to water vapor for 15 s and then left to relax for 20 s; the dynamic of the actuation is highly reproducible among different films and the difference between the maximum and the minimum bending angles is around a factor of two. To demonstrate that the NC film is able to perform a mechanical work, we loaded it by a cargo of TiO_2 nanoparticles. Different amounts of an aqueous suspension of the nanoparticles were homogeneously dispersed over the wet NC films (the details are reported in the Experimental Section). The loaded films were left to dry completely before exposing them to the water flux. We did not observe any effect of the cargo up to a TiO_2 to NC weight ratio of 1:1.

The lacking of film iridescence and of the characteristic CD features usually observed for cellulose helical structures supports the idea that no helical structures develop during the films formation. This fact might be at the origin of the mechanical flexibility of our membranes. In fact, most of the literature reports the spontaneous formation of helical structures in self-assembled NC films.[41–43] But no one has noticed the macroscopic effect we are describing here, probably because the helical structure increases the mechanical rigidity of the film.

3. Conclusion

In summary, in this paper we report the nanoscale mechanism underlying the macroscopic actuation performance of NC films induced by polar molecules. We demonstrate that NC films respond to water fluxes by a mechanical movement due to an interface-driven water sorption process. The presence of two binding sites for water within the fibril network characterized by fast and slow dynamics of exchange has been shown by spectroscopic experiments. We reported evidence that the mechanical origin of the bending is an electrostatically driven fiber extension, since the film is insensitive to nonpolar vapor molecules, while a lateral expansion of the wet film is evidenced by the AFM images and agrees with this hypothesis. Electrostatic hydrogen bonds between cellulose backbone and absorbed water molecules have been recently suggested to produce the reversible shape transitions and bending movements of films of cellulose stearoyl esters.[25] Unlike the conventional actuation mechanisms for which a relationship between stimulus amplitude and response intensity holds, the NC films transduce the difference in water fluxes magnitude into variable rate of movement. We proved that below 12 mm Hg water vapor pressures, this relationship is quantitative.

The mechanism underlying this mechanical behaviour of NC provides the basis for the design of fast and efficient actuators based on a common, renewable and biocompatible material.

4. Experimental Section

All reagents used were from Sigma (St. Louis, MO) and were used without further purification. Never dried soft bleach pulp (Celeste90) were received from SCA-Ostrand (Sweden).

Nanocellulose Film Preparation: Carboxylated NC fibers were produced by 2,2,6,6-tetramethylpiperidinyloxy (TEMPO)-mediated oxidation at alkaline condition, capable of converting primary hydroxyls into carboxylate groups.[44] 1 g of cellulose pulp was swollen in 100 mL water under stirring for 1 h. Then 0.1 g NaBr, 3.1 g NaClO, and 0.16 mg TEMPO were added under vigorous stirring. The pH of the solution was maintained in the interval 10.5-11-0 by addition of 1 M NaOH until it remained almost constant. Then the pH was lowered up to about 6.8 by washing the slurry with 400 mL high-purity water at least 20 times. 45 mL of the slurry were sonicated for 4 min at 20 KHz and 100 W_{eff} of output power delivered in the sample volume with a 13 mm diameter ultrasonic tip (Bandelin Sonopuls HD2200). This step was repeated twice and a

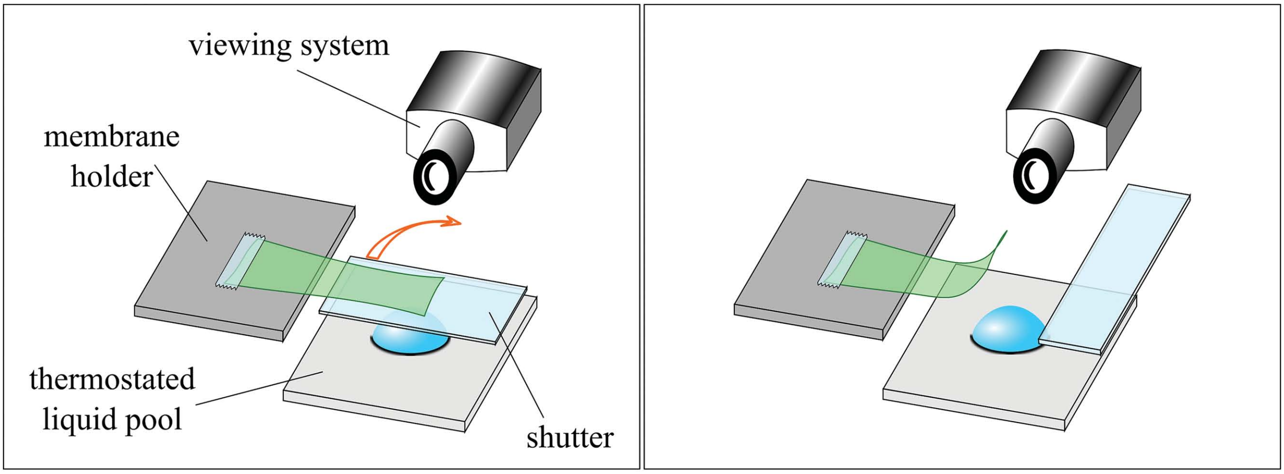

Figure 6. a) Sketch view of the setup used to measure the bending: NC film is stuck on a metallic holder and suspended over a glass slide. A drop of water is deposited beneath the shutter and is thermostated to the desired temperature. b) Upon shutter opening, evaporated water reaches the bottom surface of the film which starts to bend. The actuation is recorded with a digital camera coupled with an optical magnification system.

transparent NC suspension was obtained. After adding 50 mL distilled water, the suspension was filtered over a 1.2 μm cellulose ester Millipore filter (Merck-Millipore, Darmstdt DE) to remove residual coarse fibrils.

The films were obtained by casting the clear suspension on a Petri dish (10 cm diameter) and drying it at 60 °C in an oven over a completely flat copper foil to maintain homogeneous temperature over the whole film surface. After 24 h, the free standing transparent and homogeneous film was peeled off from the dish and conserved until use at Room Temperature (RT) in a desiccator under mild vacuum. Alternatively, the films were produced by vacuum assisted self-assembly by filtration over a 100 nm cut-off filter (Merck-Millipore). However, the casting procedure was preferred because of its simplicity and the superior quality of the obtained films.

In a typical preparation, about 1.5 mg cm^{-2} of NC (corresponding to a 10 μm film thickness) were casted, however variable thickness (in the range 5–20 μm) was obtained by casting different amounts of the starting solution.

Material Characterization: The structure of the nanofibrils was investigated using TEM. A drop of 5 μL of an aqueous NC suspension was placed on 300-mesh copper grid coated by support carbon film (Ted Pella Inc.). After 1 min excess fluid was removed, and the grids were negatively stained with 2% uranyl acetate in water for another 1 min. Samples were viewed by a FEI Tecnai 12 G2 TEM, at 120 kV.

FTIR spectra were acquired in transmission mode by a micro-FTIR Nicolet iN10 equipped with a liquid nitrogen cooled detector MCT-A. Samples were scanned in the range 750–4000 cm^{-1} with a 4 cm^{-1} resolution. The sampled area was 150 × 150 μm^2.

CD spectra were obtained with a Jasco J710 apparatus. The NC film was allocated in the cell compartment and kept stretched by a Teflon holder. The humidity level was varied by fluxing nitrogen with variable content of water vapor.

The bending of the NC film was characterized using the home-made apparatus showed in **Figure 6**: a drop of water of known volume (0.1 mL) is deposited onto a thermostated support. The NCF film is sticked on a metallic holder and a glass shutter is used to prevent any interaction between the water evaporating from the underlying drop and the NC film. A USB camera coupled to an optical magnification zoom allows the measurement of the bending of the film (spatial resolution was of about 10 μm). In all experiments, the distance between drop and shutter was fixed to 500 μm. The NC film was placed over the shutter in a flat configuration.

Loading experiments were performed by depositing on the uppermost layers of the NC films a cargo of TiO_2 nanoparticles (Aeroxide TiO_2 P25, Degussa Evonik, DE). Different volumes of a nanoparticle aqueous suspension of TiO_2 (4 mg mL^{-1}) were dispersed under gentle stirring over the wet NC films, to obtain a TiO_2/NC w/w ratio in the range 0.2/10 up to 1/1. The loaded films were dried at 60 °C and then exposed the water flux in the apparatus shown in Figure 6.

Variable Water Fluxes: Variable fluxes of gaseous water molecules at constant T were obtained by diluting water in ethylene glycol. Ethylene glycol in liquid state is miscible with water in the whole concentration range and has a negligible vapor pressure at room temperature with respect to that of water.[45] Mixtures of ethylene glycol/water in the range 0/100% up to 98/2% were prepared. The corresponding vapor pressures were calculated according to tabulated data[46] assuming that equilibrium conditions are reached at the liquid–gas interface.

Supporting Information

Supporting Information is available from the Wiley Online Library or from the author.

Acknowledgements

The research was partially funded by the Italian Ministry of University and Research through the "Futuro in Ricerca" project RBFR12OO1G – NEMATIC. The authors also acknowledge SCA Ostrand (Sweden) for the supply of the cellulose material and J. Jopp for support during the AFM measurements.

Received: July 30, 2015
Revised: November 6, 2015

---

[1] A. R. Studart, *Angew. Chem., Int. Ed.* **2015**, *54*, 2.
[2] R. J. Wojtecki, M. A. Meador, S. J. Rowan, *Nat. Mater.* **2011**, *10*, 14.
[3] C. S. Hinaes, M. D. Lima, N. Li, G. M. Spinks, J. Foroughi, J. D. W. Madden, S. H. Kim, S. Fang, M. Jung de Andrade, F. Göktepe, Ö. Göktepe, S. M. Mirvakili, S. Naficy, X. Lepró, J. Oh, M. E. Kozlov, S. J. Kim, X. Xu, B. J. Swedlove, G. G. Wallace, R. H. Baughman, *Science* **2015**, *343*, 868.
[4] H. Kim, S. Kwon, *Science* **2013**, *339*, 150.
[5] Q. Zhao, J. W. C. Dunlop, X. Qiu, F. Huang, Z. Zhang, J. Heyda, J. Dzubiella, M. Antonietti, J. Yuan, *Nat. Commun.* **2014**, *5*, 4293.

[6] X. Lu, Z. Zhang, H. Li, X. Sun, H. Peng, *J. Mater. Chem. A* **2014**, *2*, 17272.
[7] M. R. Islam, X. Li, K. Smyth, M. J. Serpe, *Angew. Chem., Int. Ed.* **2013**, *52*, 10330.
[8] J. Leng, X. Lan, Y. Liu, S. Dua, *Prog. Mater. Sci.* **2011**, *56*, 1077.
[9] S.-W. Lee, J. H. Prosser, P. K. Purohit, D. Lee, *ACS Macro Lett.* **2013**, *2*, 960.
[10] L. Ionov, *Adv. Funct. Mater.* **2013**, *23*, 4550.
[11] M. Ma, L. Guo, D. G. Anderson, R. Langer, *Science* **2013**, *339*, 186.
[12] P. K. Annamalai, K. L. Dagnon, S. Monemian, E. J. Foster, S. J. Rowan, C. Weder, *ACS Appl. Mater. Interfaces* **2014**, *6*, 967.
[13] R. M. Erb, J. S. Sander, R. Grisch, A. R. Studart, *Nat. Commun.* **2013**, *4*, 1712.
[14] T. Tanaka, *Phys. Rev. Lett* **1978**, *40*, 820.
[15] A. Muller, M. Zink, N. Hessler, F. Wesarg, F. A. Muller, D. Kralischac, D. Fischer, *RSC Adv.* **2014**, *4*, 57173.
[16] T. Shiga, Y. Hirose, A. Okada, T. Kurauchi, *J. Appl. Polym. Sci.* **1993**, *47*, 113.
[17] R. Yoshida, *Adv Mater.* **2010**, *22*, 3463.
[18] J. Dumais, Y. Forterre, *Annu. Rev. Fluid Mech.* **2011**, *44*, 453.
[19] I. Burgert, P. Fratzl, *Philos. Trans. R. Soc., A* **2009**, *367*, 1541.
[20] L. Csoka, I. C. Hoeger, O. J. Rojas, I. Peszlen, J. J. Pawlak, P. N. Peralta, *ACS Macro Lett.* **2012**, *1*, 867.
[21] J. Kim, C.-S. Song, S.-R. Yun, *Smart Mater. Struct.* **2006**, *15*, 719.
[22] G.-Y. Yuna, J. Kim, J.-H. Kim, S.-Y. Kim, *Sens. Actuators, A* **2010**, *164*, 68.
[23] A. Walther, J. V. I. Timonen, I. Díez, A. Laukkanen, O. Ikkala, *Adv. Mater.* **2011**, *23*, 2924.
[24] M. Nogi, H. Yano, *Adv. Mater.* **2008**, *20*, 1849.
[25] K. Zhang, A. Geissler, M. Standhardt, S. Mehlhase, M. Gallei, L. Chen, C. M. Thiele, *Sci. Rep.* **2015**, *5*, 11011.
[26] M. Wang, X. Tian, R. H. A. Ras, O. Ikkala, *Adv. Mater. Interfaces* **2015**, *2*, 1500080.
[27] Y. Nishiyama, *J. Wood Sci.* **2009**, *55*, 241.
[28] A. Dufresne, *Mater. Today* **2013**, *16*, 220.
[29] R. J. Moon, A. Martini, J. Nairn, J. Simonsen, J. Youngblood, *Chem. Soc. Rev.* **2011**, *40*, 3941.
[30] F. Jiang, Y.-L. Hsieh, *Carbohyd. Polym.* **2013**, *95*, 32.
[31] P. A. Giguère, K. B. Harvey, *Can. J. Chem.* **1956**, *34*, 798.
[32] J. Mann, H. J. Mariann, *Trans. Faraday Soc.* **1955**, *52*, 481.
[33] Y. Xie, C. A. S. Hill, Z. Jalaludin, S. F. Curling, R. D. Anandjiwala, A. J. Norton, G. Newman, *J. Mater. Sci.* **2011**, *46*, 479.
[34] S. Belbekhouche, J. Bras, G. Siqueira, C. Chappey, L. Lebrun, B. Khelifi, S. Marais, A. Dufresne, *Carbohyd. Polym.* **2011**, *83*, 1740.
[35] R. Kohler, R. Alex, R. Brielmann, B. Ausperger, *Macromol. Symp.* **2006**, *244*, 89.
[36] Y. Horikawa, J. Sugiyama, *Cellulose* **2008**, *15*, 419.
[37] M. Chaplin, Water structure and science, http://www1.lsbu.ac.uk/water/water_vibrational_spectrum.html (accessed: December 2015).
[38] Y. Nitta, B. S. Kim, K. Nishinari, M. Shirakawa, K. Yamatoya, T. Oomoto, Y. Asai, *Biomacromolecules* **2003**, *4*, 1654.
[39] A. Forget, J. Christensen, S. Ludeke, E. Kohler, S. Tobias, M. Matloubi, F. Thomann, V. P. Shastri, *Proc. Natl. Acad. Sci. USA* **2013**, *110*, 12887.
[40] Y. Tanaka, M. Sakurai, K. Nakamura, *Food Hydrocolloids* **1996**, *10*, 133.
[41] J. A. Kelly, C. P. K. Manchee, S. Cheng, J. M. Ahn, K. E. Shopsowitz, W. Y. Hamadc, M. J. MacLachlan, *J. Mater. Chem. C* **2014**, *2*, 5093.
[42] H. Thérien-Aubin, A. Lukach, N. Pitch, E. Kumacheva, *Nanoscale* **2015**, *7*, 6612.
[43] J. P. F. Lagerwall, C. Schutz, M. Salajkova, J. H. Noh, J. H. Park, G. Scalia, L. Bergstrom, *NPG Asia Mater.* **2014**, *6*, e80.
[44] T. Saito, S. Kimura, Y. Nishiyama, A. Isogai, *Biomacromolecules* **2007**, *8*, 2485.
[45] NIST Chemistry WebBook, http://webbook.nist.gov/cgi/cbook.cgi?Name=ethylene+glycol&Units=SI (accessed: July 2015).
[46] Union Carbide Corporation, Ethylene Glycol product guide, http://www.meglobal.biz/media/product_guides/MEGlobal_MEG.pdf (accessed: July 2015).